2023 IEEE International Conference on Robotics and Automation (ICRA 2023)
May 29 - June 2, 2023. London, UK

A Silicone-sponge-based Variable-stiffness Device

Tianqi Yue[1], Tsam Lung You[1], Hemma Philamore[1], Hermes Bloomfield-Gadêlha[1] and Jonathan Rossiter[1]

***Abstract*— Soft devices employ variable stiffness to ensure safety and improve the robustness in the interaction between robots and objects. Using soft materials is one of the most popular approaches to design a variable-stiffness device, while the use of silicone sponge remains less explored in this field. Here we present a novel silicone-sponge-based variable-stiffness device (SVD). The SVD is easy-to-make and low-cost, and fabricated by an air-tight bellow enclosing a silicone sponge core. This allows easy access to the hyper-elastic response of the porous sponge whilst stiffness tuning of the device via pneumatic pressure difference. A detailed mathematical model of the SVD is proposed, by which the stiffness can be precisely controlled by the pressure difference applied. The stiffness of SVD can be tuned in the range of $[1.55, 22.82] \times 10^3$ N/m, up to 14.7 times increase. The high stiffness is easily triggered by a low pressure difference ($\Delta P < 12$ kPa). The SVD is a versatile and compact module, with small axial size (10 mm height) and light weight (14.3 g), making it highly suitable for integration in a wide range of robotics and industrial applications. This, in addition to its easy-to-fabricate and low-cost features, may appeal to the robotics community at large. We further detail its working principle, fabrication processes, mathematical model and automated control methods to show its versatility.**

I. Introduction

Variable-stiffness devices are potential solutions for contact compliance on rigid robots to reduce damage, or for improving the load capacity of soft robots [1], [2]. To date, several variable-stiffness devices have been developed using a variety of approaches, including material jamming [2]–[9], leaf springs [10], [11], antagonistic mechanisms [12], [13] and stiffness-tunable materials such as low melting point alloys [14], [15], shape memory alloys [16], [17], electromagnet and magnetorheologic fluid [18] and thermoplastics [19]. Some designs embedded the variable-stiffness mechanism within a robotic actuator [1], [4], [10] or sensor [4] to achieve compliant actuation and perception. In addition to these material-based approaches, some researchers have used algorithmic control to actively adjust the contact force, and emulate variable stiffness in the system [20].

Jamming soft materials is an easy-to-fabricate and low-cost method to achieve variable-stiffness [2]–[9]. They are made by enclosing freely-moving materials in an elastic bag. By pumping air out of the bag, the materials are squeezed tightly which generates frictional forces to stiffen the whole bag. The features of material-jamming devices vary depending on the type of inner material used. Granular jamming shows better shape adaptation but exhibits higher weight [21], [22]. Layer jamming and fiber jamming are newer technologies and lightweight, but their applications are restricted to specific shapes, i.e., planar for layer jamming and tubular for fiber jamming [5]–[9], [23], [24]. However, the jammed state is inevitably lack of elasticity and this reduces the speed and degree of relaxation after jamming has been released. Using sponge as the filler in the bag has the lightest weight and remains a pre-defined degree of elasticity when stiffened [3], [4], since it is not indeed jammed – the open cells of the sponge collapse, storing recovery energy in the deformed elastomer, which allows the sponge to recover to its original shape when jamming is released. This makes it possible to design a silicone-sponge-based variable-stiffness device with light weight, high elasticity and fast recovery.

In this work, we propose a novel silicone-sponge-based variable-stiffness device (SVD) which is easy-to-make and shows effective tunability of its stiffness. In contrast to previous variable-stiffness devices utilizing the similar concept [3], [4], we use a rubber bellow to axially constrain its deformation and provide a precise mathematical model to achieve an accurate and fast stiffness adjustment. The SVD is formed from a cylindrical silicone sponge core enclosed

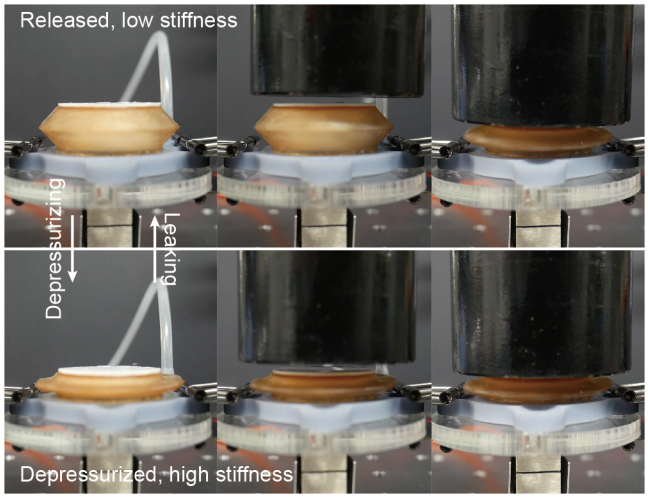

Fig. 1. The stiffness change of the SVD. Top photos: when SVD is released (air leaks), it has low stiffness. A 200 g weight compresses the SVD significantly. Bottom photos: when the SVD is compressed by pumping air out, a high stiffness is achieved. The weight does not significantly compress the SVD.

[1]Tianqi Yue, Tsam Lung You, Hemma Philamore, Hermes Bloomfield-Gadêlha and Jonathan Rossiter are with the Department of Engineering Mathematics and Bristol Robotics Laboratory at the University of Bristol, Bristol, BS8 1TW, UK {tianqi.yue, tl.you, hemma.philamore, hermes.gadelha, jonathan.rossiter}@bristol.ac.uk

TY was funded by Chinese Scholarship Council through award 201906120027. JR was supported through EPSRC research grants EP/V062158/1, EP/T020792/1, EP/V026518/1, EP/S026096/1 and EP/R02961X/1, and by the Royal Academy of Engineering as a Chair in Emerging Technologies.

Data available at: 10.5523/bris.23v6ekzwmvyop25xedxf66epjk

in a rubber bellow. The bellow is made from an elastomer with lower relative stiffness compared to the silicone sponge. By pumping air out, a pressure differential is applied to the silicone sponge and a higher stiffness is thus achieved. As shown in Fig.1 and Supplementary Video, the stiffened SVD deforms much less than the unstiffened SVD when the same compressive load is applied. A mathematical model of the SVD was built so that the stiffness of the SVD can be readily controlled by the pressure differential, which can be easy measured by a low-cost pressure sensor. We compare the two situations where a compressive force is, or is not, applied to the SVD. Based on the experimental results, the SVD can achieve the target stiffness under both conditions.

II. Structure, Concept and Modeling

The structure of the SVD is shown in Fig.2. The lid, the rubber bellow and the base form an airtight region which maintains the pressure differential. A cylindrical-shaped silicone sponge with a through-hole in the middle forms the main structure of the device and provides the majority of the stiffness of the whole device (the bellow contributes little to the total stiffness). Since the silicone sponge has an open-cell structure, air can freely flow through it. An air tube is connected to the airtight region of the SVD which is driven by an air pump. When the air pump generates a vacuum, the pressure differential $\Delta P = P_{\text{atm}} - P_{\text{in}}$ increases, where P_{in} and P_{atm} are the inner pressure and the atmospheric pressure. The pressure differential applied to the SVD compresses the silicone sponge. In contrast to other material-jamming devices that enclose the filling materials entirely by an elastic bag (e.g., a balloon), the SVD uses a rubber bellow with low axial stiffness but relative high radial stiffness. Under the pressure differential, the rubber bellow only interacts with the silicone sponge core in the axial direction, minimizing its radial interference. The larger the pressure differential, the stiffer the silicone sponge becomes. The three diagrams on the right of Fig.2 show this process. When the pressure differential reaches the maximum P_{max}, the stiffest state is achieved. When air is permitted to flow back into the bellow, the pressure differential gradually returns to zero due to the elasticity, and stored elastic energy, of the silicone sponge.

The SVD utilizes the non-linear hyper-elasticity property of silicone to realize variable stiffness. However, solid silicone cannot be used due to its rapid increase in stiffness with compression. A compression test of a solid silicone and a silicone sponge of the same dimensions was conducted and their compression properties are compared in Fig.3. For solid silicone (illustrated by the red line), the stiffness K (i.e., the slope) increases very fast with the increase of compressive distance d. It is difficult to exploit the variable stiffness of the solid silicone in such a small compression range ($0 \sim 60$ N). By adding pores into the solid silicone, the silicone sponge shows a much shallower stiffness increase (blue line) than the solid silicone. This is because the open-cell structure provides a mild stiffness increase as the cells collapse during compression. When the cells are nearly fully collapsed, the stiffness rapidly increases to that of solid silicone. This

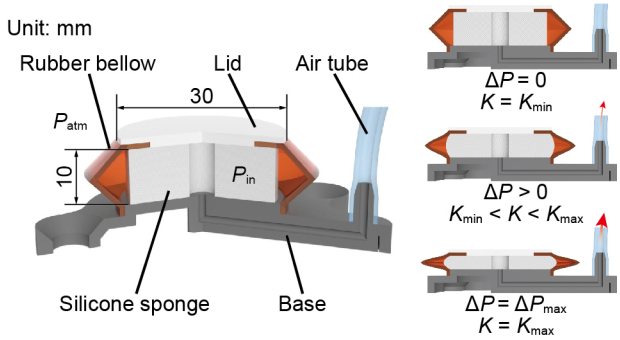

Fig. 2. Structure of the SVD. The top lid (white, rigid), rubber bellow (amber, soft) and the base (grey, rigid) form an airtight region. The air tube is connected to a pneumatic pump. Initially, the inner pressure and atmosphere are balanced and the stiffness is at minimum (top right). When pumping air out, the silicone sponge is gradually compressed by the pressure differential force, resulting in significant increase in stiffness (middle right). When the pressure differential reaches a maximum, the stiffness of the SVD achieves its maximum (bottom right).

property endows the silicone sponge with a much larger tunable range of stiffness as shown in Fig.3 (shaded region). Theoretically, stiffness is equal to the slope of the curve of compressive force F against compressive distance d, i.e.,

$$K(d) = \lim_{\Delta d \to 0} \frac{F(d + \Delta d) - F(d)}{\Delta d}.$$

However, in the practical situation we consider, Δd is not zero. In this paper, we set $\Delta d = 1$ mm when measuring K for all the following modelling and discussions of the SVD. In Fig.3, this estimated stiffness is indicated by the slopes in black diagonal dashed lines as an example. d can be adjusted by applying a pressure differential to the silicone sponge. For example, when the SVD is applied by a small pressure differential ΔP_1 as Fig.3 shows, the stiffness is determined by $K_{1,\text{ sponge}} = \Delta F_1 / \Delta d_1$. When SVD is applied by a larger pressure differential ΔP_2, the stiffness is determined by $K_{2,\text{ sponge}} = \Delta F_2 / \Delta d_2$ to achieve a larger stiffness (note that $\Delta d_1 = \Delta d_2 = 1$ mm). Therefore, the stiffness K can be controlled by the pressure differential. The open cells of silicone sponge allow air to freely flow through the silicone sponge which makes this pneumatically-controlled variable-stiffness device simple, robust and fast acting. The tunable region will be explained in the modelling part below.

The fabrication of SVD is straightforward. The top lid and the bottom base are 3D printed from printable resin (Photon Mono X, Anycubic). The rubber bellow is cast from soft polyurethane rubber (PT Flex 50, Polytek) with 1 mm wall thickness. The silicone sponge is made by the following steps. First, mix liquid silicone (Dragon Skin$^{\text{TM}}$ 10 NV, Smooth-on) part A and part B by a mass ratio of 1:1 and stir thoroughly. Second, weight table salt, with mass 4 times that of the liquid silicone. Add salt to the mixed liquid silicone and thoroughly stir. Third, cast the mixture in a mold until it is cured ($\sim$ 2 hours in a 40$^{\text{o}}$C oven). Fourth, remove the cured silicone from the mold and soak it in water in order to dissolve the salt granules ($\sim$ 2 days). Finally, dry the silicone sponge and use a hole puncher (diameter of 5 mm) to make a

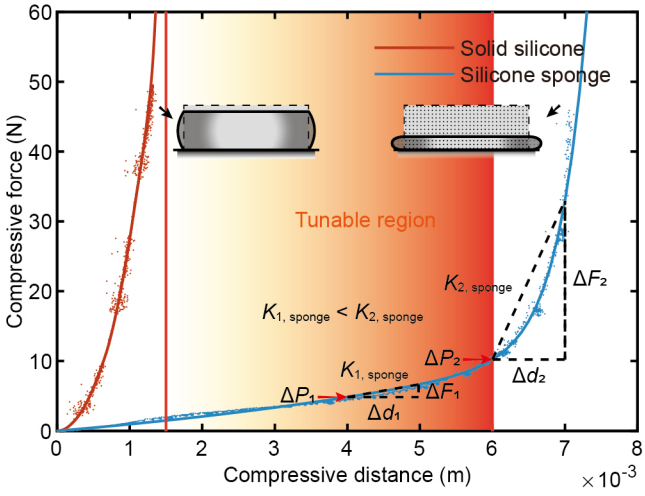

Fig. 3. Measured mechanical properties of solid silicone and silicone sponge under compression. The two pieces of silicone are of the same dimensions of $\varnothing 28 \times 10$ (diameter $\times$ height, mm) with a through-hole ($\varnothing 5$ mm) in the middle, both are formed from Dragon Skin$^{\text{TM}}$ 10 NV. During compression, the stiffness of the solid silicone increases rapidly, which made its stiffness difficult to control. The silicone sponge, however, has a larger compression range and lower stiffness gradient. When applying pressure differential ($\Delta P_1 < \Delta P_2$), the silicone sponge achieved different stiffnesses. The tunable stiffness region is selected as $[1.5, 6] \times 10^{-3}$ m.

through-hole in the middle of the sponge. This hole provides a path for the rapid flow of air into and out of the sponge. The lid, the rubber bellow and the base are bonded using super glue (Loctite), and the silicone sponge is fixed inside the bellow using silicone glue (Sil-Poxy$^{\text{TM}}$, Smooth-on).

We build the mathematical model of the SVD by the following analysis. The force balance of the SVD is always:

$$F + F_{\text{p}}(d, \Delta P) = F_{\text{s}}(d) + F_{\text{b}}(d),$$

where F is a known downward compressive force, $F_{\text{p}}(d)$ is the pressure-induced downward compressive force, $F_{\text{s}}(d)$ is the counterforce from the compressed silicone sponge and $F_{\text{b}}(d)$ is the counterforce from the compressed rubber bellow. d is the compressive distance of the top lid, which is measured downwards from the original position. The force balance diagram is shown in Fig.4. $F_{\text{p}}(d)$ is expressed by

$$F_{\text{p}}(d, \Delta P) = \Delta P \cdot \pi r_{\text{b}}^2(d) = (P_{\text{atm}} - P_{\text{in}}) \cdot \pi r_{\text{b}}^2(d),$$

where $r_{\text{b}}(d)$ is the radius of the bellow corner, as Fig.4 shows. Therefore, the pressure differential ΔP can be expressed in terms of the compressive distance d by:

$$\Delta P = \frac{F_{\text{s}}(d) + F_{\text{b}}(d) - F}{\pi r_{\text{b}}^2(d)}. \tag{1}$$

To obtain $r_{\text{b}}(d)$ we used simulation (COMSOL Multiphysics). In the simulation, we assumed $\Delta P = 0$ kPa and therefore the bellow was only affected by the compressive force from the top lid. The simulation result showed $r_{\text{b}}(d) = 0.41d + 0.02$ as shown in Fig.4. In reality, r_{b} will also be affected by ΔP since the bellow will deform under the pressure differential. Here we use $r_{\text{b}}(d)$ as a first approximation to establish the model and will modify it subsequently. ΔP can be calculated by solving Eq.(1). Next, we will discuss the relation between stiffness K and d. Once the $\Delta P : d$ and $d : K$ relations have both been determined, K can be obtained from ΔP. Since stiffness is defined by $K(d) = [F(d + \Delta d) - F(d)]/\Delta d$, it can be divided into components:

$$K(d) = \frac{\Delta F(d)}{\Delta d} = K_{\text{s}}(d) + K_{\text{b}}(d) + K_{\text{p}}(d, \Delta P),$$

where $K_{\text{s/b/p}}(d) = \Delta F_{\text{s/b/p}}(d)/\Delta d$ are the stiffnesses induced by the silicone sponge, the rubber bellow and the sealed air, respectively. We assume that $F_{\text{s}}(d)$ and $F_{\text{b}}(d)$ are only related to the compressive distance d and can be easily measured by compression tests. The measured F_{s} and F_{b} are fitted well by exponential fitting as follows:

$$F_{\text{s}}(d) = 5.97(e^{148.4d} - 1) + 2.89 \times 10^{-7}(e^{2593d} - 1),$$
$$F_{\text{b}}(d) = -0.9755(e^{-444d} - 1) - 0.9752(e^{-444d} - 1).$$

$F_{\text{s}}(d)$ is the blue line drawn in Fig.3. The fitted function matches the recorded data well when $d \in [0, 7]$ mm. Since we let $\Delta d = 1$ mm, we selected $d = 6$ mm as the upper limit for the tunable stiffness region. F_{b} is not drawn in Fig.3 since it is much smaller than $F_{\text{s}}(d)$ thus influences very little to the total stiffness. Based on $F_{\text{s/b}}(d)$, $K_{\text{s/b}}(d)$ can be obtained by $K_{\text{s/b}} = [F_{\text{s/b}}(d + 1 \times 10^{-3}) - F_{\text{s/b}}(d)]/(1 \times 10^{-3})$. K_{p} is expressed by,

$$\begin{aligned} K_{\text{p}}(d, \Delta P) =& \frac{F_{\text{p}}(d + \Delta d, \Delta P(d + \Delta d)}{\Delta d} \\ & - \frac{F_{\text{p}}(d, \Delta P(d)))}{\Delta d} \\ =& \frac{\pi r_{\text{b}}^2(d + \Delta d)[P_{\text{atm}} - P_{\text{in}}(d + \Delta d)]}{\Delta d} \\ & - \frac{\pi r_{\text{b}}^2(d)[P_{\text{atm}} - P_{\text{in}}(d)]}{\Delta d}. \end{aligned}$$

Since the bellow is sealed when the air pump stops working, the inner gas follows the ideal gas law:

$$P_{\text{in}}(d + \Delta d) - P_{\text{in}}(d) = \frac{[V(d) - V(d + \Delta d)]P_{\text{in}}(d)}{V(d + \Delta d)},$$

where V is the sealed air volume in the bellow. Since the calculation of the true V is too complicated, we estimate V by assuming the inner volume of the bellow is the sum of two symmetrically-placed cones:

$$V(d) = \frac{\pi}{3}(1 \times 10^{-2} - d)[r_{\text{l}}^2 + r_{\text{b}}^2(d) + r_{\text{l}} r_{\text{b}}(d)].$$

Based on the experimental results in the following section, the error caused by the approximation is negligible. $P_{\text{in}}(d) = 101$ kPa is taken as the critical condition into calculation since the air-induced stiffness in the system reaches its maximum under this situation. Substituting all the known

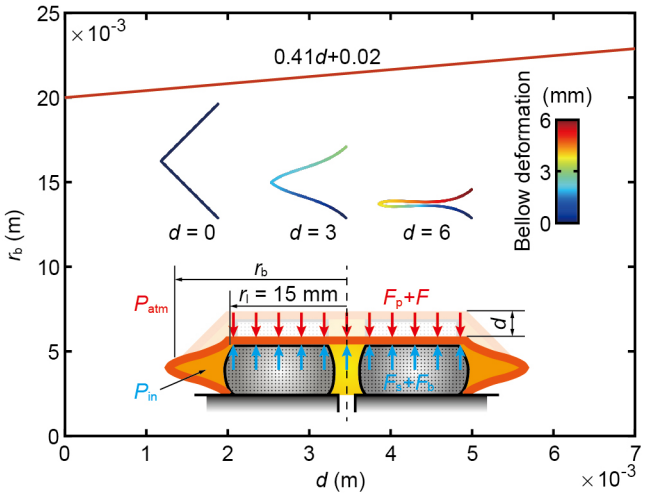

Fig. 4. The mathematical model of the SVD. Curve: the simulation results of $d : r_{\mathrm{b}}$ relation. Middle insets: simulated rubber bellow edge deformation with respect to d change. Bottom inset: the force balance diagram of SVD when a known downward compressive force F is applied and a pressure differential is maintained.

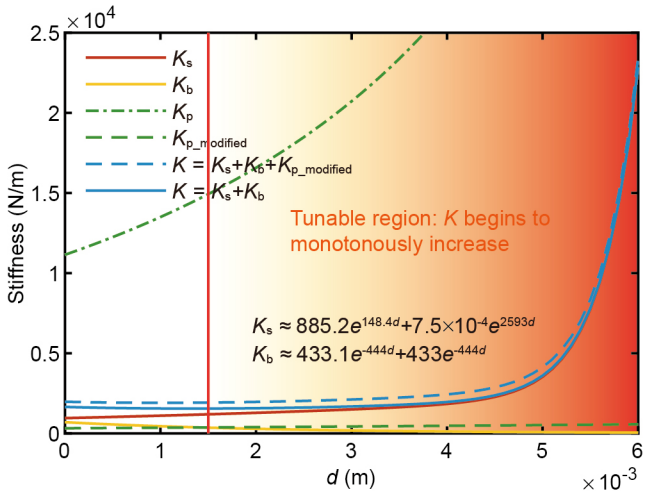

Fig. 5. The stiffness calculation of the SVD. In the tunable region, the calculated stiffness K monotonously increases from $K_{\mathrm{min}}(d = 1.5\mathrm{mm}) = 1.55 \times 10^3$ N/m to $K_{\mathrm{max}}(d = 6\ \mathrm{mm}) = 22.82 \times 10^3$ N/m. Without the air reservoir, K_{p} is too large compared to $K_{\mathrm{s/b}}$. After the addition of the reservoir, $K_{\mathrm{p\_modified}}$ is negligible, which can be seen by the small interval between $K = K_{\mathrm{s}} + K_{\mathrm{b}} + K_{\mathrm{p\_modified}}$ and $K = K_{\mathrm{s}} + K_{\mathrm{b}}$.

parameters, we compare K_{p} with K_{s} and K_{b} in Fig.5. This shows that K_{p} dominates the total stiffness. However, we want K_{s} to dominate the total stiffness and K_{p} to be negligible. To address this problem, an air reservoir (made by an airtight glass bottle) with a volume of 3×10^{-4} m^3 was connected to the pneumatic system in series. The inner air volume then increases to

$$V(d) = \frac{\pi}{3}(1 \times 10^{-2} - d)[r_{\mathrm{l}}^2 + r_{\mathrm{b}}^2(d) + r_{\mathrm{l}} r_{\mathrm{b}}(d)] + 3 \times 10^{-4}.$$

The influence of $K_{\mathrm{p\_modified}}$ is now negligible which is demonstrated by the small interval between the blue dashed line ($K = K_{\mathrm{s}} + K_{\mathrm{b}} + K_{\mathrm{p}}$) and blue solid line ($K = K_{\mathrm{s}} + K_{\mathrm{b}}$) in Fig.5. Therefore, $K = K_{\mathrm{s}} + K_{\mathrm{b}}$ is used for the following discussions. Note that, this small interval caused by neglecting K_{p} is calculated by considering the critical condition. In practical applications, this interval will be even smaller for most cases. K decreases from $d = 0$ mm then begins to monotonously increase when $d \geq 1.5$ mm. Therefore, $d \in [1.5, 6]$ mm is selected as the stiffness tunable region. The minimum stiffness was found to be $K_{\mathrm{min}}(d = 1.5\mathrm{mm}) = 1.55 \times 10^3$ N/m and the maximum stiffness $K_{\mathrm{max}}(d = 6\ \mathrm{mm}) = 22.82 \times 10^3$ N/m, which is a 14.7 times increase.

The former $\Delta P : d$ relation is an approximation used for estimating the air-induced stiffness, which ignores the impact of ΔP on r_{b}. To verify its correctness, we measured the practical $\Delta P : d$ relation and plotted it in Fig.6. We used two different weights, 200 g and 500 g, to generate three cases when compressive forces $F = 0$, 2 and 5 N. By increasing the pressure differential from 0 kPa to 35 kPa with an interval of 5 kPa, the top lid displacement was measured. Note that this displacement (plotted in circular markers in Fig.6) is measured by regarding the position after the weight has been stably placed as zero, rather than by calculating compressive distance from the original undeformed shape (plotted in dashed lines). Fig.6 shows that the pressure differential cannot generate a compressive distance d as large as that modelled. In other words, the former estimated $r_{\mathrm{b}}(d)$ is larger than the practical case. We observed that the pressure differential squeezed the bellow wall towards the center, which decreased the bellow corner radius. This deformation is highly non-linear and not the focus of this work, therefore we use curve fitting to give a rational approximation of $r_{\mathrm{b}}(d, \Delta P)$:

$$r_{\mathrm{b}}(d, \Delta P) = a\Delta P^b(0.41d + 0.02),$$

where $a = -1.22$, $b = -0.0444$ are the fitted parameters. The top lid displacement calculated by the modified $r_{\mathrm{b}}(d, \Delta P)$ (solid lines in Fig.6) shows good agreement with the experimental results in all F situations. Therefore, this relation is used in the following experiments.

III. Experimental Results

The experimental setup is shown in Fig.7. An Arduino UNO board is used to control the system. A linear stage driven by a stepper motor is mounted vertically on an experimental metal breadboard to move a flat PMMA sheet (5 mm thickness) upward and downward. The motor is driven by a micro stepper driver (DM542) and is controlled by the microcontroller. Between the PMMA sheet and linear slider, a load cell (DYLY-106) is mounted in the middle for measuring the compressive force, via a signal amplifier (RW-ST01A) to the microcontroller. The SVD is mounted below the PMMA sheet on the breadboard. An air pump (ZX512-503-2900N), a pressure sensor (BMP280, BOSCH), a three-way solenoid valve and a reservoir (3×10^{-4} m^3) are connected in series to SVD, thereby sharing the same inner pressure. The air pump is used for pumping air out

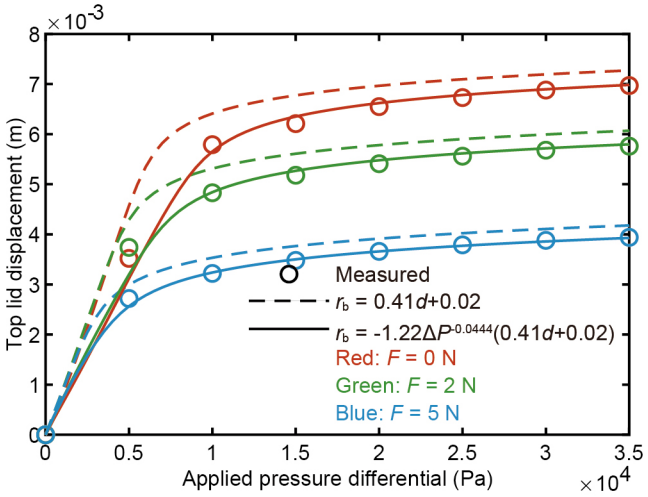

Fig. 6. The characterization of pressure-induced displacement. Zero displacement is set as $\Delta P = 0$ kPa when the weight is stably placed on the top lid. By taking the effect of ΔP into consideration of r_b, the modified curves (solid lines) show good agreement with experimental data (circular markers), while the unmodified curves show overestimated displacement.

while the solenoid valve is used to balance the overshooting. A needle valve is connected to the solenoid valve to reduce the air leakage rate. A laser displacement sensor (LK-G402, Keyence) is used to measure the vertical displacement of the PMMA sheet via a signal amplifier (LK-GD500) to the microcontroller. The feedback data, including the external force F, the compressive displacement d and the pressure differential ΔP are acquired by the microcontroller at the same interval (typically 10 ms).

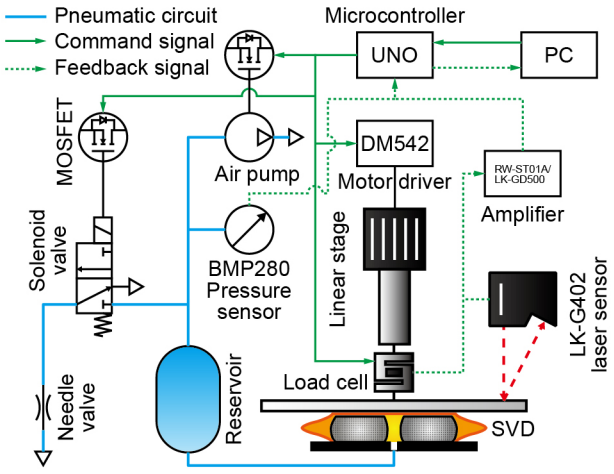

Fig. 7. The experimental setup.

Two experiments were implemented to verify the stiffness model. In the first experiment, external force $F = 0$ N was set. This simulates the situation where the contact force is initially zero (e.g., touch, collision, etc.). The second experiment set the compressive force $F \neq 0$ N. This is for simulating the situation when the device is holding a non-zero force against an object and a specific stiffness is required (e.g., force-controlled polishing, moving objects, etc.). For $F = 0$ N experiments, we selected the target stiffnesses $[K_{\min}, K_{\text{mid}}, K_{\max}] = [1.55, 12, 22.82] \times 10^3$ N/m (the minimum stiffness, the middle stiffness and the maximum stiffness repectively) derived by the mathematical model. $[\Delta P_{\min}, \Delta P_{\text{mid}}, \Delta P_{\max}] = [2.45, 10.25, 11.72]$ kPa were calculated by substituting $F = 0$ N into modified Eq.(1). The experiments were implemented as follows. 1) The air pump pumped air out of the SVD until the pressure differential exceeded the desired value. 2) The needle valve opened to let air slowly in until the pressure differential stabilized at the desired value. 3) The linear stage moved the load cell and the PMMA sheet downward to compress the SVD. The laser displacement sensor monitored the PMMA sheet displacement. When the contact force became non-zero, the corresponding position was recorded as the starting position and the linear stage moved down for a further 1 mm. 4) After the compression, the linear stage reset to its initial position and the d, F data was recorded. The stiffness K was calculated by the d, F data in the 1 mm compression range.

The results of the $F = 0$ N experiments are shown in Fig.8. ΔF is calculated by the increase from the first to the end of the 1 mm compression. The measured stiffness (dash-dotted lines) matched the calculated stiffness (black dashed lines) well for $K_{\min}$ and K_{mid}, while $K_{\max}$ shows a small deviation. This might be caused by the shape deformation of the PMMA sheet under a high compressive force. Overall, the experimental results show good agreement with the mathematical model.

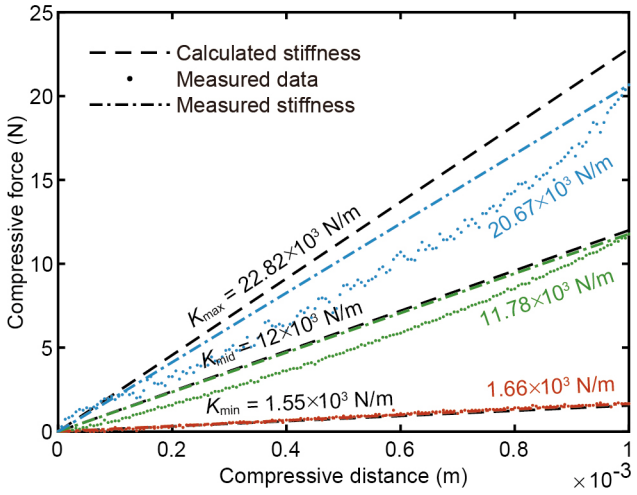

Fig. 8. The experimental results of $F = 0$ N experiments. Three stiffness were achieved by adjusting the pressure differentials to the calculated values, demonstrating the accuracy of the mathematical model when $F = 0$ N.

For $F \neq 0$ N situation, we selected $F = [3, 8]$ N as the compressive forces. From the mathematical model, we know that the maximum stiffnesses with respect to different compressive forces are the same, which is $K_{\max} = 22.82 \times 10^3$ N/m. However, the minimum stiffnesses for different F are different since any $F \neq 0$ N causes a pre-

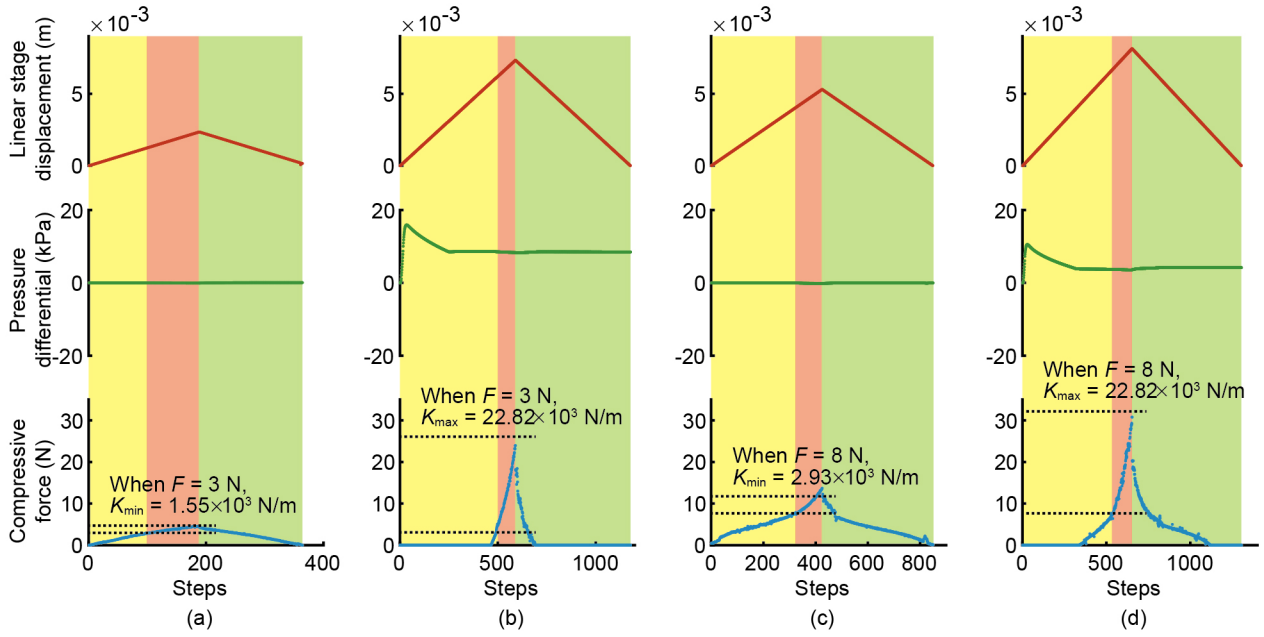

Fig. 9. The experimental results of $F \neq 0$ N experiments. From (a) to (d): $K_{\min}(F = 3\text{ N})$, $K_{\max}(F = 3\text{ N})$, $K_{\min}(F = 8\text{ N})$ and $K_{\max}(F = 8\text{ N})$. Yellow, red and green regions: PID tuning period, 1 mm compression period and resetting period, respectively. The x label "Steps" indicates the number of data acquisition samples recorded by the microcontroller.

compressed d. For the test, the minimum stiffnesses were calculated by substituting $F = [3, 8]$ N and $\Delta P_{\min} = [0, 0]$ kPa into the mathematical model. $K_{\min}$ were then derived as $[1.55, 2.93] \times 10^3$ N/m. The pressure differentials required to obtain maximum stiffnesses were calculated as $\Delta P_{\max} = [8.56, 3.53]$ kPa. The $F \neq 0$ N experiments were implemented as follows. 1) The air pump worked to degas until the pressure differential went below the desired (calculated) value, then the needle valve opened to slowly let air in. In the meantime, the linear stage moved downward and began to contact the SVD. The contact force was adjusted by a PID controller. 2) The linear stage began to move downward for 1 mm until both the pressure differential and the compressive force were adjusted to the desired values. 3) The linear stage reset back to its initial position and the d, ΔP, F data were recorded.

The experimental results of $F \neq 0$ N are shown in Fig.9. Fig.9 (a) to Fig.9 (d) are the data recorded in the tests of $K_{\min}(F = 3\text{ N})$, $K_{\max}(F = 3\text{ N})$, $K_{\min}(F = 8\text{ N})$ and $K_{\max}(F = 8\text{ N})$. The yellow, red and green regions reflect the period when the system is being tuned to the desired state by the PID controller, the 1 mm compression test period and the resetting period, respectively. After both the compressive force and pressure differential were tuned to the target value (lower dashed lines in Fig.9 (a-d)), all the final forces obtained by compressing the SVD for 1 mm were near the predicted value (upper dashed lines). The slightly larger stiffness recorded in the third test ($K_{\min}(F = 8\text{ N})$), was caused by neglecting the air-induced stiffness as discussed in section II. These results show a large and predictable tunable stiffness range under compression.

IV. Conclusion

In this work, we present a novel design for realising a facile, low-cost and effective silicone-sponge-based variable-stiffness device (SVD). The SVD is made by enclosing a cylinder of silicone sponge in a rubber bellow, then adjusting the stiffness by applying a pressure differential to the bellow. The stiffness of the SVD is dominated by the non-linear stiffness of the silicone sponge core, therefore controlling a pressure differential tunes the stiffness. The mathematical model of the SVD is established and verified by experiments. In this work, up to 14.7 times stiffness increase is achieved by applying a pressure differential below 12 kPa. Larger stiffness increases can be realised by a higher pressure differential. This will be the topic of future work. Here we demonstrated that the SVD is capable of adjusting its stiffness whether loaded or not.

The SVD is robot-friendly due to its light weight (14.3 g, pneumatic system not included) and small size (10 mm height). The compression properties of the silicone sponge can be engineered by changing the silicone hardness and the salt-silicone mass ratio during fabrication. The compressive force and displacement range can be modified by adjusting the dimensions of the SVD. Therefore, it can be used at the end of a robotic arm with engineerable properties for adapting to different applications. Limits of the SVD can be: 1) The inherent hysteresis effect of silicone and rubber, and 2) The coupled displacement and stiffness change (which is a common issue of variable-stiffness devices). These are also our future focuses. We believe this silicone-sponge-based variable-stiffness device will provide a novel solution in industry and healthcare, for example, tunable-stiffness requirement on robotic polishing and ultrasound imaging.

REFERENCES

[1] S. Wolf, G. Grioli, O. Eiberger, W. Friedl, M. Grebenstein, H. Höppner, E. Burdet, D. G. Caldwell, R. Carloni, M. G. Catalano, *et al.*, "Variable stiffness actuators: Review on design and components," *IEEE/ASME transactions on mechatronics*, vol. 21, no. 5, pp. 2418–2430, 2015.

[2] W. Dou, G. Zhong, J. Cao, Z. Shi, B. Peng, and L. Jiang, "Soft robotic manipulators: Designs, actuation, stiffness tuning, and sensing," *Advanced Materials Technologies*, vol. 6, no. 9, p. 2100018, 2021.

[3] M. A. Robertson and J. Paik, "New soft robots really suck: Vacuum-powered systems empower diverse capabilities," *Science Robotics*, vol. 2, no. 9, p. eaan6357, 2017.

[4] J. Peters, B. Anvari, C. Chen, Z. Lim, and H. A. Wurdemann, "Hybrid fluidic actuation for a foam-based soft actuator," in *2020 IEEE/RSJ International Conference on Intelligent Robots and Systems (IROS)*. IEEE, 2020, pp. 8701–8708.

[5] Y. Li, M. Cong, D. Liu, Y. Du, M. Wu, and C. W. de Silva, "Development of a novel robotic hand with soft materials and rigid structures," *Industrial Robot: the international journal of robotics research and application*, 2021.

[6] X. Zeng, C. Hurd, H.-J. Su, S. Song, and J. Wang, "A parallel-guided compliant mechanism with variable stiffness based on layer jamming," *Mechanism and Machine Theory*, vol. 148, p. 103791, 2020.

[7] Y.-J. Kim, S. Cheng, S. Kim, and K. Iagnemma, "A novel layer jamming mechanism with tunable stiffness capability for minimally invasive surgery," *IEEE Transactions on Robotics*, vol. 29, no. 4, pp. 1031–1042, 2013.

[8] M. Brancadoro, M. Manti, F. Grani, S. Tognarelli, A. Menciassi, and M. Cianchetti, "Toward a variable stiffness surgical manipulator based on fiber jamming transition," *Frontiers in Robotics and AI*, vol. 6, p. 12, 2019.

[9] S. Jadhav, M. R. A. Majit, B. Shih, J. P. Schulze, and M. T. Tolley, "Variable stiffness devices using fiber jamming for application in soft robotics and wearable haptics," *Soft Robotics*, vol. 9, no. 1, pp. 173–186, 2022.

[10] J. Wu, Z. Wang, W. Chen, Y. Wang, and Y.-h. Liu, "Design and validation of a novel leaf spring-based variable stiffness joint with reconfigurability," *IEEE/ASME Transactions on Mechatronics*, vol. 25, no. 4, pp. 2045–2053, 2020.

[11] M. K. Shepherd and E. J. Rouse, "Design of a quasi-passive ankle-foot prosthesis with biomimetic, variable stiffness," in *2017 IEEE international conference on robotics and automation (ICRA)*. IEEE, 2017, pp. 6672–6678.

[12] Z. Fang, C. Huang, Y. Wang, J. Xu, J. Tan, B. Li, Z. Wang, Y. Wu, A. Huang, J. Yi, *et al.*, "Multi-dimensional proprioception and stiffness tuning for soft robotic joints," in *2022 International Conference on Robotics and Automation (ICRA)*. IEEE, 2022, pp. 10 973–10 979.

[13] K. Althoefer, "Antagonistic actuation and stiffness control in soft inflatable robots," *Nature Reviews Materials*, vol. 3, no. 6, pp. 76–77, 2018.

[14] J. Shintake, B. Schubert, S. Rosset, H. Shea, and D. Floreano, "Variable stiffness actuator for soft robotics using dielectric elastomer and low-melting-point alloy," in *2015 IEEE/RSJ International Conference on Intelligent Robots and Systems (IROS)*. IEEE, 2015, pp. 1097–1102.

[15] H. Abidi, A. Tonazzini, M. Cianchetti, D. Floreano, and A. Menciassi, "Low melting point alloy based stiffening of a soft robot," in *International Congress of the Society for Medical Innovation and Technology*, 2017.

[16] W. Wang and S.-H. Ahn, "Shape memory alloy-based soft gripper with variable stiffness for compliant and effective grasping," *Soft robotics*, vol. 4, no. 4, pp. 379–389, 2017.

[17] W. Wang, C. Y. Yu, P. A. Abrego Serrano, and S.-H. Ahn, "Shape memory alloy-based soft finger with changeable bending length using targeted variable stiffness," *Soft robotics*, vol. 7, no. 3, pp. 283–291, 2020.

[18] Y. Okatani, T. Nishida, and K. Tadakuma, "Development of universal robot gripper using mrα fluid," in *2014 Joint 7th International Conference on Soft Computing and Intelligent Systems (SCIS) and 15th International Symposium on Advanced Intelligent Systems (ISIS)*. IEEE, 2014, pp. 231–235.

[19] M. C. Yuen, R. A. Bilodeau, and R. K. Kramer, "Active variable stiffness fibers for multifunctional robotic fabrics," *IEEE Robotics and Automation Letters*, vol. 1, no. 2, pp. 708–715, 2016.

[20] C. Zeng, H. Su, Y. Li, J. Guo, and C. Yang, "An approach for robotic leaning inspired by biomimetic adaptive control," *IEEE Transactions on Industrial Informatics*, vol. 18, no. 3, pp. 1479–1488, 2021.

[21] T. Ranzani, M. Cianchetti, G. Gerboni, I. De Falco, and A. Menciassi, "A soft modular manipulator for minimally invasive surgery: design and characterization of a single module," *IEEE Transactions on Robotics*, vol. 32, no. 1, pp. 187–200, 2016.

[22] I. De Falco, M. Cianchetti, and A. Menciassi, "A soft multi-module manipulator with variable stiffness for minimally invasive surgery," *Bioinspiration & biomimetics*, vol. 12, no. 5, p. 056008, 2017.

[23] T. Wang, J. Zhang, Y. Li, J. Hong, and M. Y. Wang, "Electrostatic layer jamming variable stiffness for soft robotics," *IEEE/ASME Transactions on Mechatronics*, vol. 24, no. 2, pp. 424–433, 2019.

[24] S. G. Fitzgerald, G. W. Delaney, and D. Howard, "A review of jamming actuation in soft robotics," in *Actuators*, vol. 9, no. 4. MDPI, 2020, p. 104.